ORIGINAL ARTICLE

Failure mechanisms in single-point incremental forming of metals

Maria B. Silva · Peter S. Nielsen · Niels Bay · P. A. F. Martins

Abstract The last years saw the development of two different views on how failure develops in single-point incremental forming (SPIF). Today, researchers are split between those claiming that fracture is always preceded by necking and those considering that fracture occurs with suppression of necking. Each of these views is supported by convincing experimental and theoretical arguments that are available in the literature. This paper revisits failure in SPIF and presents a new level of understanding on the influence of process variables such as the tool radius that assists the authors to propose a new unified view on formability limits and development of fracture. The unified view conciliates the aforementioned different explanations on the role of necking in fracture and is consistent with the experimental observations that have been reported in the past years. The work is performed on aluminium AA1050-H111 sheets and involves independent determination of formability limits by necking and fracture using tensile and hydraulic bulge tests in conjunction with SPIF of benchmark shapes under laboratory conditions.

Keywords Single-point incremental forming · Failure · Experimentation

M. B. Silva · P. A. F. Martins (✉)
IDMEC, Instituto Superior Tecnico, TULisbon,
Av. Rovisco Pais,
1049-001 Lisbon, Portugal
e-mail: pmartins@ist.utl.pt

P. S. Nielsen · N. Bay
Department of Mechanical Engineering,
Technical University of Denmark,
DTU—Building 425,
2800 Kgs. Lyngby, Denmark

Notation

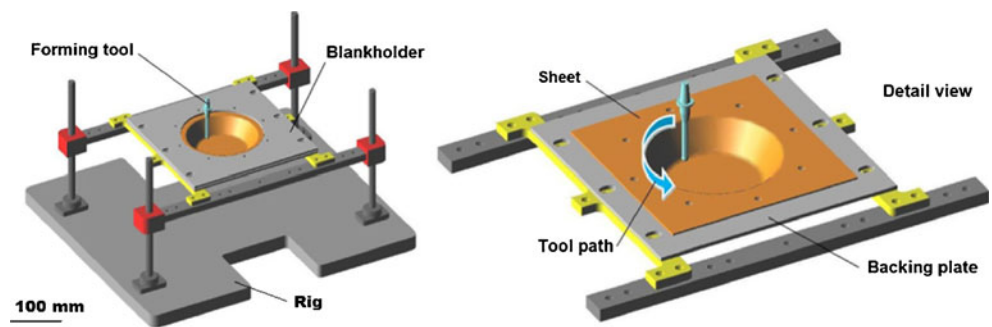|	
ε	True strain
σ	True stress
σ_θ	Circumferential stress
σ_ϕ	Meridional stress
σ_t	Thickness stress
σ_Y	Yield stress
ψ	Draw angle between the inclined wall and the initial flat configuration of the sheet
ψ_{max}	Maximum admissible draw angle between the inclined wall and the initial flat configuration of the sheet
t	Thickness of the sheet
r_{tool}	Radius of the SPIF tool
r_{part}	Radius of the SPIF part
r_{part}/r_{tool}	Incremental tool ratio

1 Introduction

In single-point incremental forming (SPIF), a sheet is clamped rigidly around its edges but unsupported underneath and formed by a hemispherical-ended forming tool, which describes the contour of the desired geometry. The process is schematically drawn in Fig. 1 and includes the following components: (a) the sheet metal blank, (b) the blankholder, (c) the backing plate and (d) the rotating single-point forming tool. The tool path is generated in a computer-aided manufacturing programme and is utilised to progressively form the sheet into a component.

The timeline of the investigation in SPIF of metallic materials can be divided into two different periods. During the early years of development, most studies on SPIF have concerned capabilities of using special purpose [1] or

ordinary computer numerical control machine tools [2, 3], development of laboratory applications and experimental characterization of the formability limits in terms of the major fundamental process parameters [4]. During this period of time, the mechanics of deformation and the physics behind failure remained little understood. The consensus was that formability limits in SPIF were much higher than those found in conventional stamping, but the explanation was unclear and often attributed to the localization of plastic deformation, to the sine law or to the spinnability relation due to Kegg [5], which gives emphasis to the importance of axis-parallel shear as in case of shear spinning. More recently, there has been considerable research effort allocated to understand the deformation mechanics of SPIF in terms of its major parameters with the objective of identifying the typical modes of deformation, explaining the mechanisms that enable deformation above the forming limit curve (FLC) and establishing the formability limits across the useful range of operating conditions.

As with all new processes, there has been a number of approaches to fulfil the aforementioned objective, and as a result of these efforts, there are different views and considerable debate on the likely mode of failure and governing mode of deformation in SPIF. The state-of-the-art review paper by Emmens and van den Boogaard [6] presents an excellent overview of the most significant contributions with special emphasis on the mechanisms that have been proposed to explain plastic deformation above the FLC.

On the contrary to Emmens and van den Boogaard that classified different research contributions on the basis of the proposed mechanisms and their ability to avoid, postpone or reduce the growth rate of necking in SPIF, authors decided to follow a broader systematization procedure built upon the existence or avoidance of necking before failure. As a result of this, research contributions were classified in two different groups: (a) the 'necking view' (NV) and (b) the 'fracture view' (FV). Researchers supporting the NV consider (a) that formability is limited by necking, (b) that the FLC in SPIF is significantly raised against conventional FLCs being utilised in the analysis of sheet metal forming

processes (e.g. deep drawing and stretch forming) [3] and (c) that the raise in formability is due to a stabilizing effect caused by large amount of through thickness shear [7, 8] or by serrated strain paths arising from cyclic, local plastic deformation [9].

Researchers supporting the FV [10–12] consider (a) that formability is limited by fracture without experimental evidence of previous necking, (b) that the suppression of necking in conjunction with the low growth rate of accumulated damage is the key mechanism for ensuring the high levels of formability in SPIF and (c) that FLCs that give the loci of necking strains are not relevant and should be replaced by the fracture forming limits (FFLs).

As recently shown by Silva et al. [13], the FV has strong arguments against failure being limited by previous necking because experimental results confirm that forming limits can be approximated, in the principal strain space, by straight lines with negative slopes on the form $\varepsilon_1 + \varepsilon_2 = q$ placed well above conventional FLCs and in line with FFLs. Moreover, if through thickness shear or serrated strain paths arising from cyclic, local plastic deformation, could be capable of increasing the forming limits of AA1050-O to a level of approximately six times of that experimentally found by means of tensile, elliptical and circular bulge tests [14], this would mean that the individual stabilizing effect of stresses and strain paths of SPIF on the FLCs would be much larger than in conventional sheet metal forming processes. This is not only difficult to justify on the basis of the localized nature of plastic deformation but suffers from lack of experimental evidence (as pointed out in [6]).

However, the experimental results on SPIF of pyramid test shapes with tools having different diameters obtained by Bambach and Hirt [15] can be utilised as a counter-argument against the FV. In fact, if the concept of the failure being limited by fracture without experimental evidence of previous necking requires that all possible fracture strains are located on a specific line (FFL), which is exclusively dependent on material properties [16], how can the forming limits presented in Fig. 2 of [15] show significant sensitivity to the radius of the tooling (3, 5 and 15 mm)? In particular, why is the forming limit

Fig. 2 Fracture forming limit diagram containing the forming limit curve (*FLC*) and the fracture forming limit line (*FFL*) for the aluminium AA1050-H111 with 1 mm of thickness
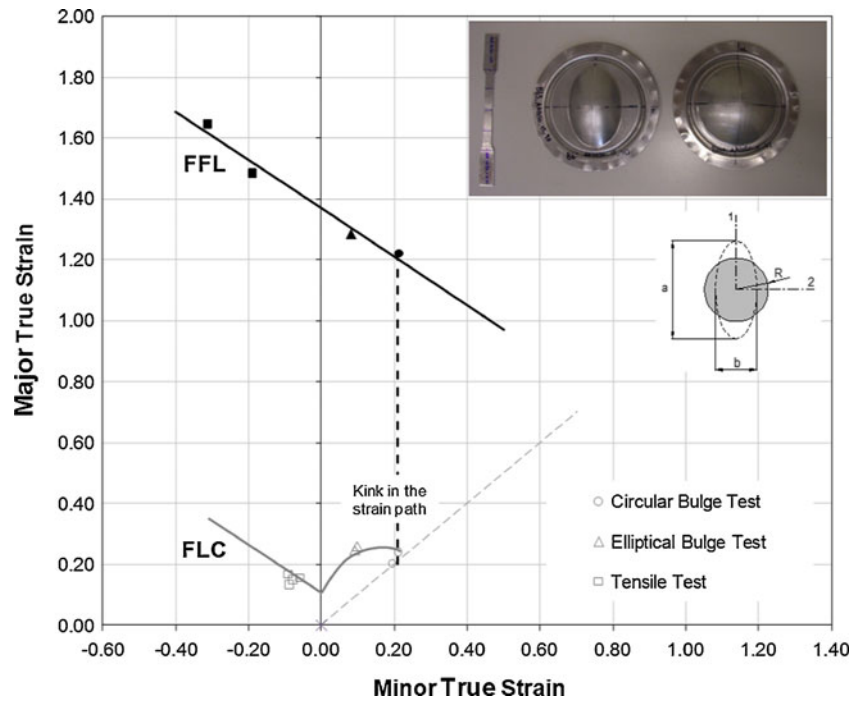
obtained by means of a tool with a radius of 3 mm much higher than those obtained with tools having radius of 5 and 15 mm? These questions need to be properly addressed.

But the abovementioned paper also provides an interesting set of results obtained from SPIF of four different test shapes (straight, cross, hyperbola and flower) made from a 1-mm thickness DC04 steel sheet with a single-point forming tool having a large radius of 15 mm. In fact, the observation that all but the hyperbola shape show pronounced necking before fracture is a strong counter-argument against the FV and does not match the observations of other researchers that claim failure to be limited by fracture without evidence of previous necking.

All these contradictions make the present authors wonder if the understanding on the mechanism of failure in SPIF is being pushed back to the starting line or, alternatively, if the likely mode of failure (fracture with or without evidence of previous necking) may be dependent on process parameters such as the sheet thickness, tool diameter, lubrication conditions and material properties, as suggested in the conclusions of the review paper by Emmens and van den Boogaard [6].

This paper seeks to examine these issues by means of an experimental investigation comprising independent determination of forming limits by necking and fracture and testing of benchmark SPIF parts under laboratory conditions. The work is performed on aluminium AA1050-H111 sheets with 1 mm thickness and the radius of the tool varied from 4 to 25 mm in order to examine its influence on the failure mechanisms. The new contribution to knowledge derives from putting forward an explanation for failure in

SPIF that is capable of closing the missing link between claims of failure being limited by previous necking (NV) or by fracture with suppression of necking (FV).

2 Experimentation

This section starts by describing the techniques that were utilised for obtaining the material forming limits by necking (FLC) and fracture (FFL) and follows by identifying the process parameters and presenting the experimental work plan prepared for investigating the failure mechanisms in SPIF.

2.1 Material forming limits

All the specimens were made from AA1050-H111 sheet blanks with 1 mm thickness. Formability was evaluated by means of tensile tests (using specimens cut at 0°, 45° and 90° with respect to the rolling direction) and bi-axial, circular (100 mm) and elliptical (100/63 mm) hydraulic bulge tests (Fig. 2).

The technique utilised for obtaining the FLC involved electrochemical etching of a grid of circles with 2 mm initial diameter on the surface of the sheets before forming and measuring the major and minor axis of the ellipses that result from the plastic deformation of the circles during the formability tests. The values of strain were computed from (refer to the detail in Fig. 2),

$$\varepsilon_1 = \ln\left(\frac{a}{2R}\right) \quad \varepsilon_2 = \ln\left(\frac{b}{2R}\right) \tag{1}$$

where the symbol R represents the original radius of the circle and the symbols a and b denote the major and minor axis of the ellipse.

The resulting FLC is plotted in Fig. 2 and was constructed by taking the principal strains $(\varepsilon_1, \varepsilon_2)$ at failure from grid-elements placed just outside the neck (that is, adjacent to the region of intense localization) since they represent the condition of the uniformly thinned sheet just before necking occurs [17].

The intersection of the FLC with the major strain axis is found to occur at $\varepsilon_1 = 0.07$ in fair agreement with the value of the strain hardening exponent of the stress–strain curve obtained by means of tensile tests,

$$\sigma = 140\,\varepsilon^{0.041}\ \text{MPa} \tag{2}$$

The experimental FFL is more difficult to obtain than the FLC. Application of grids even with very small circles in order to obtain strains in the necking region after it forms and, therefore, close to the fracture provides strain values that cannot be considered the fracture strains. Moreover, such grids create measurement problems and suffer from sensitivity to the initial size of the circles used in the grids due to the inhomogeneous deformation in the neighbour-hood of the crack.

As a result of this, the experimental procedure for constructing the FFL required measuring of thickness before and after fracture at several places along the crack in order to obtain the 'gauge length' strains. The strain in the width direction was obtained differently for tensile and bulge tests. In case of tensile tests, measurements were directly taken from the width of the specimens whereas in case of bulge tests, measurements required the utilisation of the imprinted grid of circles in order to obtain the initial and deformed reference lengths. The procedures are illustrated in Fig. 3.

The third fracture strain component, in the plane of the sheet with direction perpendicular to the crack, was determined by volume constancy knowing the two other strains. The strains at the onset of fracture are plotted in Fig. 2, and the FFL is approximated by a straight line $\varepsilon_1 + 0.79\varepsilon_2 = 1.37$

falling from left to right in good agreement with the condition of constant thickness strain at fracture (given by a slope of '−1') proposed by Atkins [18].

The large distance between neck formation (FLC) and collapse by fracture (FFL) indicates that AA1050-H111 is a very ductile material that allows a considerable through-thickness strain between neck initiation and fracture. As seen in Fig. 2, at the onset of local instability implying transition from the FLC representing necking towards the FFL, a sharp bend occurs in the strain path when testing is done with conventional bulge tests. The strain paths of bi-axial circular and elliptical bulge formability tests show a kink after neck initiation towards vertical direction, corresponding to plane strain conditions, as schematically plotted by the grey dashed line for the circular bulge formability test. The strain paths of tensile formability tests also undergo a significant change of strain ratio from slope −2 to a steeper one although not to vertical direction. The absence of a sharp kink of the strain path into vertical direction in formability testing in tension but a less abrupt bend instead is due to the fact that major and minor strains after the onset of necking do not coincide with the original pulling direction. A comprehensive analysis on the direction of the strain paths in the tension-compression strain quadrant can be found in the work of Atkins [16, 18].

2.2 Single-point incremental forming

In a previous work recently published by the authors [10], the mechanics of deformation of SPIF was modelled by means of an analytical framework developed under the theory of membrane with bi-directional in-plane contact friction forces. The framework assumed plastic deformation in the small contact area between the tool and the part of the sheet placed immediately ahead as a combination of three fundamental modes of deformation: (a) plane strain stretching on flat surfaces, (b) plane strain stretching on rotational symmetric surfaces and (c) equal bi-axial stretching on corners.
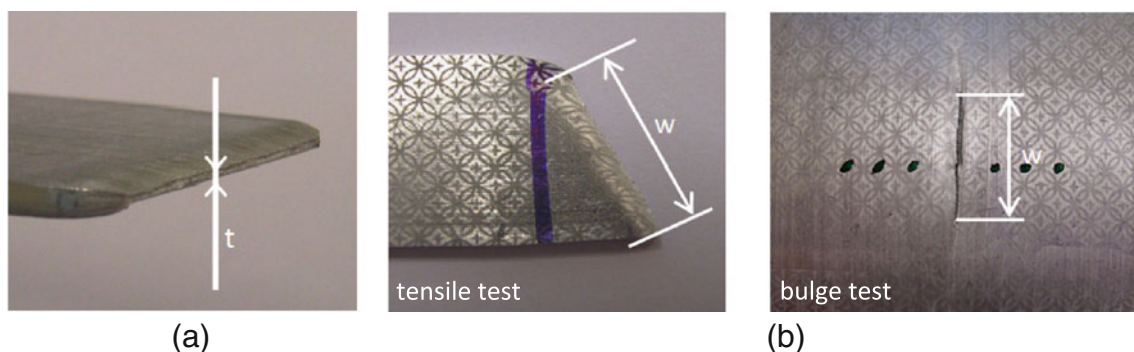

(a)   (b)

Fig. 3 Experimental procedures that were utilised for obtaining the experimental values of strain along the **a** thickness and the **b** width directions at the onset of fracture (FFL)

Table 1 presents the states of strain and stress that are derived from the analytical framework of SPIF [10] and helps identifying the process parameters as the thickness of the sheet t, the radius of the tool r_{tool} and the stress–strain response of the material (or the yield stress σ_Y in case of a rigid-perfectly plastic material). The lubrication conditions between the tool and the sheet play an important role in final surface quality of the SPIF parts [19], but the influence of friction in the overall formability of the process is negligible [13].

The experiments were performed in a Cincinnati Milacron machining centre equipped with a rig, a backing plate, a blankholder for clamping the sheet metal blanks and a rotating, single-point forming tool (Fig. 1). The blank size was 250×250 mm, the speed of rotation was 35 rpm and the feed rate was 1,000 mm/min. The tool path was helical with a step size per revolution equal to 0.5 mm, and the lubricant applied between the forming tool and the sheet was diluted cutting fluid.

The experiments were aimed at examining the influence of process parameters on failure mechanisms, namely on the occurrence of fracture with or without evidence of previous necking. However, instead of designing the experiments to cover all possible combinations of process parameters, it was decided to keep thickness of the sheet and material properties unchanged and only vary the radius of the tool. This is because the thickness of the sheet is generally only allowed to vary within a relatively narrow band (say, between 0.5 and 3 mm) and because the material is in most cases imposed by the application.

Five different single-point forming tools with radius varying from 4 to 25 mm (Fig. 4) and hemispherical tips were made of cold working tool steel (120WV4-DIN)

hardened and tempered to 60 HRc in the working region to allow the plan of experiments listed in Table 2. The experimental methodology consisted in measuring the strain values at different locations along the meridional direction from laboratory SPIF tests performed in truncated conical and pyramidal shapes characterized by stepwise varying drawing angles ψ with the depth (Fig. 5). Circle grids with 2-mm-diameter circles were electrochemically etched on the surface of the sheets in order to allow the principal strains to be measured following the procedure described in Section 2.1. The strains at the onset of fracture were obtained from the circles placed immediately adjacent to the crack. The experiments were done in random order and at least two replicates were produced for each combination of thickness and geometry in order to provide statistical meaning.

3 Results and discussion

The first part of this section examines the maximum drawing angle and the outcome of circle grid analysis in the principal strain space. The second part is focused on the analysis of thickness variation along the meridional cross section of truncated conical and pyramidal SPIF parts. The combination of results is utilised to demonstrate the influence of tool radius on failure mechanisms, namely in the existence or suppression of necking before fracture.

3.1 Maximum drawing angle

The experimental results included in Fig. 6 show the influence of the tool radius r_{tool} on the maximum drawing

Table 1 State of stress and strain in the small localized contact region between the tool and the sheet placed immediately ahead
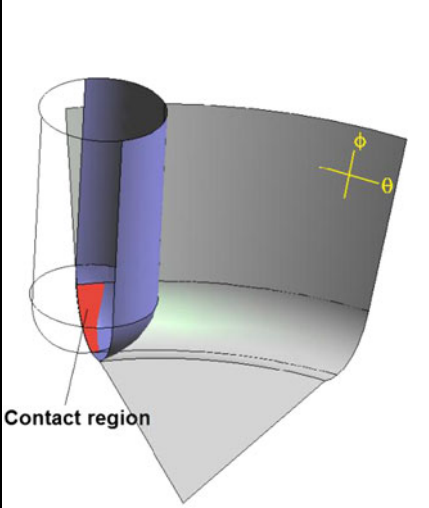

| | **Plane strain conditions** (flat and rotational symmetric surfaces) | $d\varepsilon_\varphi = -d\varepsilon_t > 0$ $d\varepsilon_\theta = 0$ $d\varepsilon_t < 0$ | $\sigma_\varphi = \sigma_1 = \dfrac{\sigma_Y}{(1 + t/r_{tool})} > 0$ $\sigma_\theta = \sigma_2 = \frac{1}{2}(\sigma_1 + \sigma_3)$ $\sigma_t = \sigma_3 = -\sigma_Y \dfrac{t}{(r_{tool} + t)} < 0$ |
| | **Equal bi-axial stretching** (corners) | $d\varepsilon_\varphi = d\varepsilon_\theta > 0$ $d\varepsilon_t < 0$ | $\sigma_\varphi = \sigma_\theta = \sigma_1 = \dfrac{\sigma_Y}{(1 + 2t/r_{tool})} > 0$ $\sigma_t = \sigma_3 = -2\sigma_Y \dfrac{t}{(r_{tool} + 2t)} < 0$ |

Fig. 4 The five different single-point forming tools that were utilised in the experiments. The tools have hemispherical tips and their radius varies from 25 mm (*leftmost*) to 4 mm (*rightmost*)

angle ψ_{max}. Three different regions can be distinguished. The left region (labelled 'A') shows that the largest values of the maximum drawing angle ψ_{max} are attained for the smallest tool radius. This observation is in close agreement with the state of stress obtained from the analytical framework developed by the authors [10] because the decrease in tool radius r_{tool} accounts for a significant decrease in the triaxiality ratio σ_m/σ_Y and, therefore, to an increase in the overall formability (refer to Tables 1 and 3).

The middle region (labelled 'B'), which will later be seen as necessary for ensuring a smooth transition where failure progressively evolves from existence to s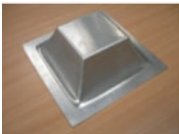uppression of necking, is a region where the maximum drawing angle ψ_{max} continues to present significant variations with the tool radius. These variations are more pronounced in the case of pyramids and, therefore, formability decays more rapidly for the pyramids than for the cones. This result is in close agreement with the computed evolution of the triaxiality ratio with the tool radius plotted in Fig. 6 that predicts larger growing rates for equal bi-axial stretching than for plane strain conditions inside region 'B'.

Finally, in the right region (labelled 'C') of Fig. 6, not only the maximum drawing angle ψ_{max} is insensitive to tool radius but measured values are identical for cones and pyramids. While results in region 'C' may at first sight be considered surprising and incoherent because the triaxiality ratio growths monotonically with tool radius and its values in equal bi-axial stretching are up to 20% larger than in plane strain conditions, they make sense if changes in failure mechanisms are to be considered. In fact, the experimental results seem to indicate that failure by fracture with suppression of necking may not be the failure mechanism suitable for all testing conditions. In particular, the results found in region 'C' unveil the possibility of failure being controlled by an alternative mechanism whenever larger tool radius are employed. This will be further investigated in the sections below.

3.2 Circle grid analysis and material forming limits

The experimental distribution of the major and minor true strains obtained from circle grid analysis in the

Table 2 The plan of experiments showing the main operating parameters and the number of parts produced for each test case

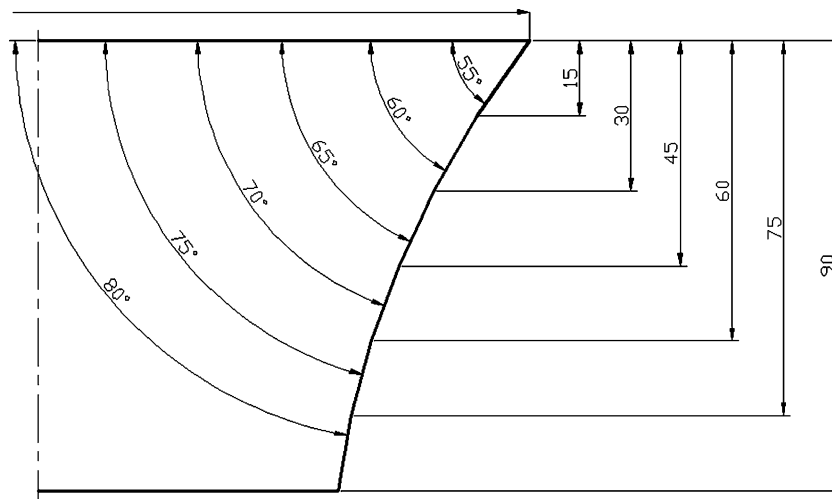| Geometry	Sheet thickness	Feed rate	Tool radius				
			4 mm	6 mm	10 mm	15 mm	25 mm
Truncated conical shape	1 mm	1,000 mm/min	2	2	2	2	2
Truncated pyramidal shape	1 mm	1,000 mm/min	2	2	2	2	2

Fig. 5 Geometry of a cross section of the truncated conical and pyramidal shapes

principal strain space is presented in Figs. 7 and 8. Results confirm that truncated conical shapes are formed under plane strain conditions while truncated pyramidal shapes are obtained under bi-axial stretching in the corners and plane-strain conditions in the side walls. It is worth to notice that the experimental values of fracture strains for the pyramids are not placed on the equal bi-axial strain ratio line with slope +1 in the principle strain space. In fact, although the onset of failure is located at corners of the pyramids, the values of fracture strains are somewhat deviating towards the plane strain direction. This also explains the existence of different values of fracture strains plotted at various locations of the first quadrant of the principal strain space.
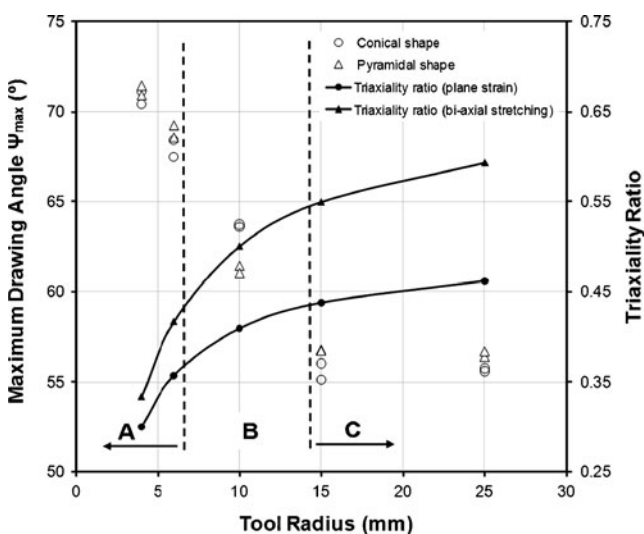
The black solid line, denoted as 'FFL', is the fracture forming line, and the grey solid line, denoted as 'FLC', is the forming limit curve obtained from experimental tensile and bi-axial bulge tests (refer to Section 2.1). The FFL is bounded by a grey area corresponding to an interval of 10% due to the experimental uncertainty in its determination.

The agreement between the FFL and the experimental fracture strains measured for the conical and pyramidal SPIF parts produced with tools having radius equal to 4 and 6 mm is very good. However, the experimental fracture strains obtained for the SPIF parts produced with larger tools exhibit considerable deviations from the FFL, which become more significant as the tool radius increases.

The abovementioned deviations for the SPIF parts produced with larger tools are in line with the observations of Bambach and Hirt [15] who concluded that limiting fracture strains are sensitive to tool radius. This is a solid argument against the assumption of a unique failure mechanism solely based on fracture with suppression of necking because the FFL is supposed to be a material dependent line, insensitive to loading paths [16].

3.3 Wall thickness

Figure 9 shows the evolution of the wall thickness along the meridional cross section of truncated pyramids produced with tools having five different radius. Top and bottom figures are related with measurements taken in cross sections parallel and perpendicular to the rolling direction, respectively.

As seen in both Fig. 9a, b, there are two completely different patterns. In case of SPIF with tools having small radius (4, 6 and 10 mm), variation of thickness with depth reveals that plastic deformation takes place by uniform

Fig. 6 Maximum drawing angle ψ_{max} and triaxiality ratio σ_m/σ_Y as a function of the tool radius for SPIF of truncated conical and pyramidal shapes

Table 3 Triaxiality ratio σ_m/σ_Y for plane strain and equal bi-axial stretching conditions

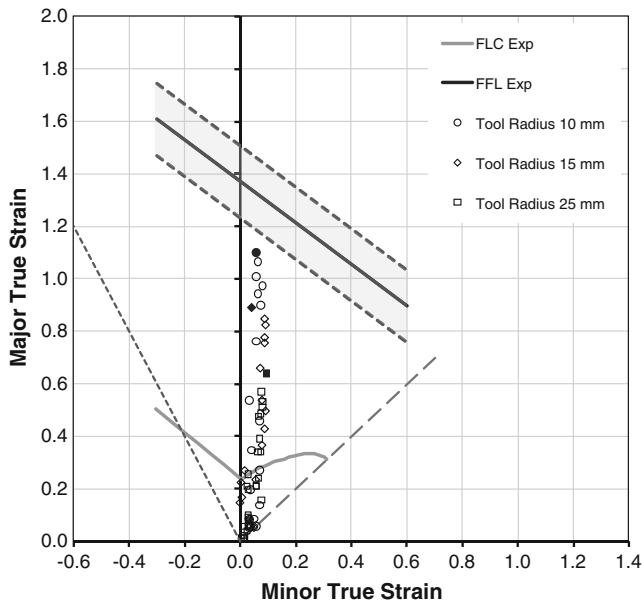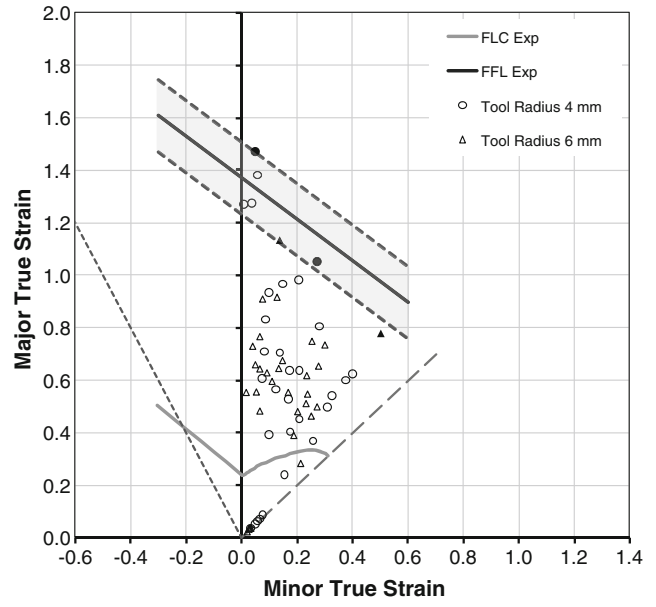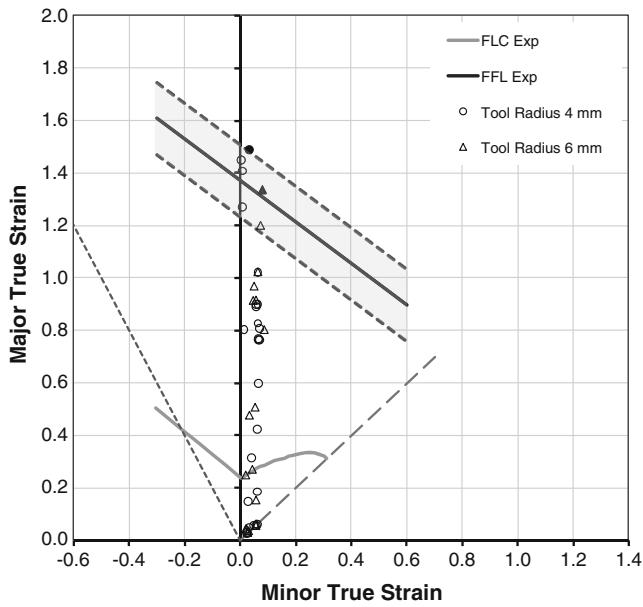|	Hydrostatic stress	Thickness (mm)	Tool radius (mm)	$\frac{t}{r_{tool}}$	$\frac{\sigma_m}{\sigma_Y}$
Plane strain conditions	$\sigma_m = \frac{\sigma_Y}{2}\left[\frac{r_{tool}-t}{r_{tool}+t}\right]$	1	4	0.250	0.30
		1	6	0.167	0.36
		1	10	0.100	0.41
		1	15	0.067	0.44
		1	25	0.040	0.46
Equal bi-axial stretching	$\sigma_m = \frac{2\sigma_Y}{3}\left[\frac{r_{tool}-t}{r_{tool}+2t}\right]$	1	4	0.250	0.33
		1	6	0.167	0.42
		1	10	0.100	0.50
		1	15	0.067	0.55
		1	25	0.040	0.59
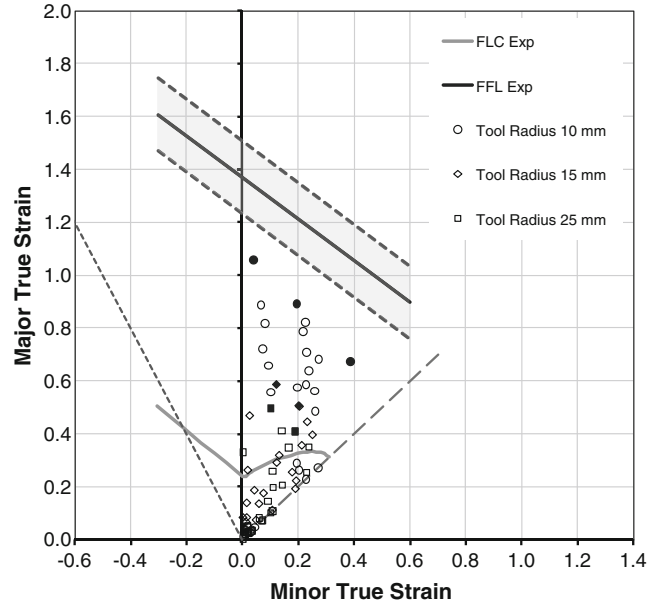
Fig. 7 Experimental strains obtained in SPIF of truncated conical shapes with tools having different radius. The *solid marks* correspond to fracture points

Fig. 8 Experimental strains obtained in SPIF of truncated pyramidal shapes with tools having different radius. The *solid marks* correspond to fracture points

Fig. 9 Variation of wall thickness with depth for truncated pyramidal shapes produced by SPIF with tools having different radius: **a** measurements along the meridional cross-sectional parallel to the rolling direction of the truncated pyramid parts. **b** Measurements along the meridional cross-sectional perpendicular to the rolling direction of the truncated pyramid parts
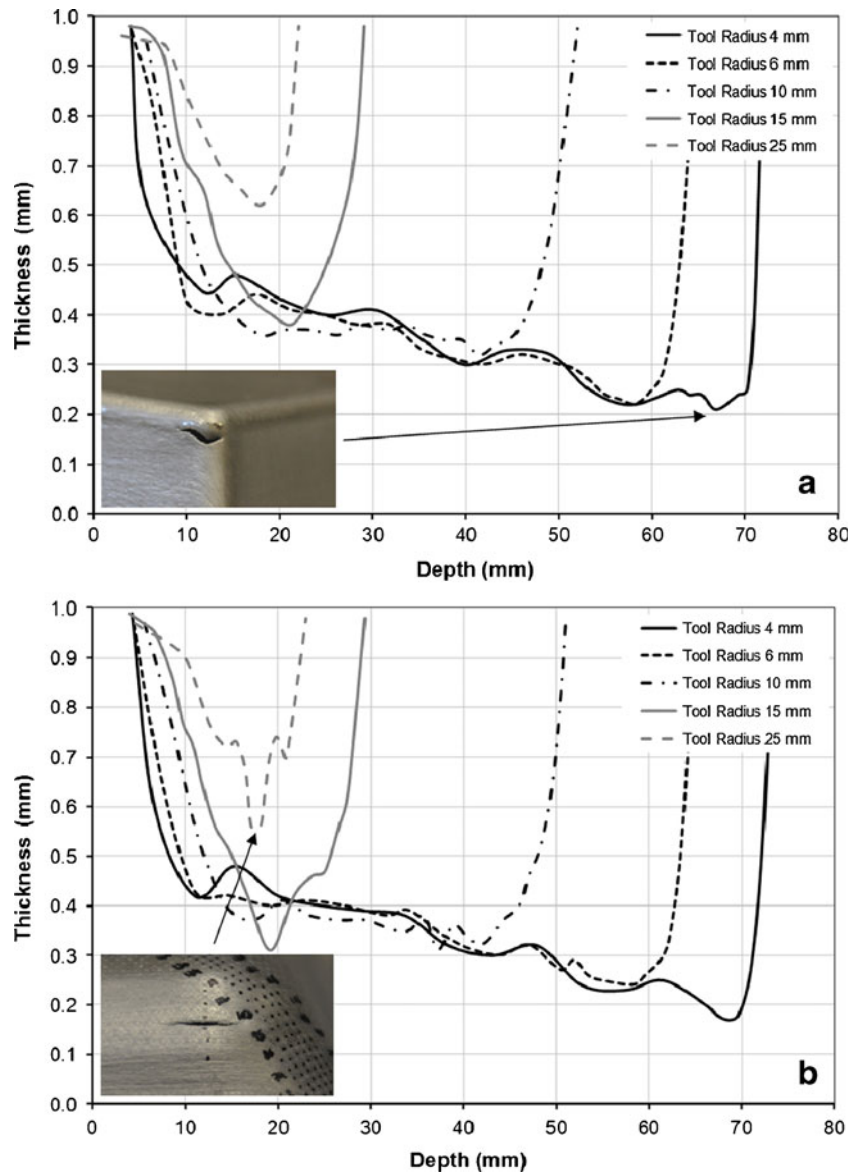

thinning until fracture. In other words, there is no experimental evidence of localized necking taking place before reaching the onset of fracture. This is in close agreement with previous observations by the authors [10] and confirms that suppression of necking is the key mechanism that together with the low growth rate of accumulated damage is capable of ensuring the high levels of formability found in SPIF with tools having small radius. In fact, if a neck was to form at the small plastic deformation zone in contact with an incremental forming tool having a small radius, it would have to grow around the circumferential bend path that circumvents the tool. This is difficult and would create problems of neck development because, even if the conditions for localized necking could be met at the small plastic deformation zone in contact with the tool, growth

would be inhibited by the surrounding material which experiences considerably lower levels of stresses.

However, in case of SPIF with tools having larger radius (15 and 25 mm), the variation of thickness with depth presents a sharp drop towards fracture that is typical of necking and localization of plastic deformation. This result is consistent with what is currently observed in stamping, which can be seen as an extreme case of SPIF where the radius of the tool r_{tool} is identical to the radius of the part r_{part}.

In case of SPIF of truncated conical shapes, the sharp decrease of the incremental tool ratio r_{part}/r_{tool} with the radius of the tool that is observed in Fig. 10 confirms fracture with previous necking (refer to 'B' in Fig. 10) when the differences in neighbouring plastically deforming regions are negligible, just like in conventional stamping.

Fig. 10 Incremental tool ratio (r_{part}/r_{tool}) as a function of tool radius r_{tool} for the SPIF of truncated conical shapes showing two different types of failure; **a** fracture with suppression of necking and **b** fracture with previous necking
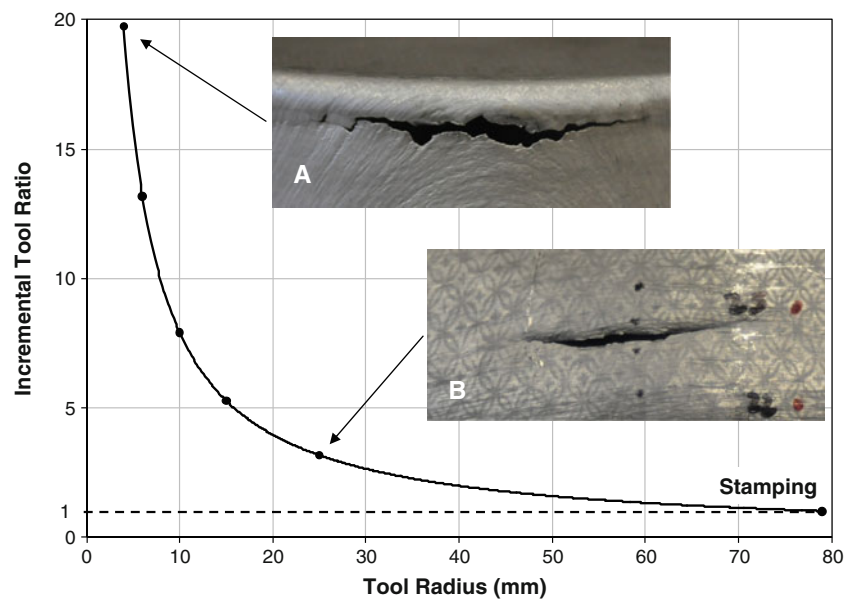
Conversely picture 'A' in Fig. 10 shows that large values of the incremental tool ratio r_{part}/r_{tool} are likely to promote fracture with suppression of necking in close agreement with what is commonly found in the SPIF of pyramids with tools having small radius (refer to the picture enclosed in Fig. 9a).

In between, the two aforementioned mechanisms there must be a transition zone where failure progressively evolves from existence to suppression of necking. Because the existence of necking in SPIF requires conventional FLCs to be raised beyond what is expected from the simple strain paths found in SPIF of cones and pyramids, it is necessary to consider additional explanations. A possible explanation considers that dynamic bending-under tension (BUT) typical of incremental forming processes gives rise to a stabilizing effect that is proportional to the ratio t/r_{tool} between the sheet thickness and the radius of the tool [6].

Combining the stabilizing effect due to dynamic BUT [6, 20] with the experimental observations performed by the authors, it is possible to propose the existence of a critical threshold for the ratio t/r_{tool} that separates fracture with previous necking from that with suppression of necking. For small ratios of t/r_{tool} (e.g. large tool radius), the stabilizing effect will be capable of raising the FLC above what is commonly found in stamping in order to allow localization by necking whereas for large ratios of t/r_{tool} (e. g. small tool radius), the stabilizing effect will not be sufficient to ensure localization and, as a result of this, failure mechanism will change to promote fracture with suppression of necking. Failure by fracture with suppression of necking is commonly observed in SPIF with tools having standard radius, and the limiting fracture strains are governed by the FFL in the principal strain space [10]. The proposed new explanation for the mechanisms of failure in

SPIF is intended to close the link between claims of failure being limited by fracture with previous necking (NV) or by fracture with suppression of necking (FV) and ensures consistency with the results that were made available in the literature for the past couple of years.

4 Conclusions

This paper presents a new insight in SPIF that helps to characterize development and propagation of fracture in the light of a unified view that is capable of including claims of existence and suppression of necking. The new proposed explanation is supported by a comprehensive experimental investigation on the influence of tool radius in the development of necking and determination of formability limits in the principal strain space.

The research work allowed identifying a critical threshold for the ratio between the thickness of the sheet and the radius of the tool that distinguishes between fracture with and without previous necking. For large tool radius, the stabilizing effect of dynamic bending under tension seems to be capable of raising the forming limit curve above what is commonly found in stamping in order to ensure localization by necking. For small tool radius, the stabilizing effect is not sufficient to ensure localization, and as a result of this, failure mechanism will change in order to promote fracture with suppression of necking. As claimed by the authors in a previous investigation [10], failure by fracture with suppression of necking is governed by the fracture forming line in the principal strain space and is the key mechanism of SPIF with tools having standard radius.

References

1. Kitazawa K, Wakabayashi A, Murata K, Yaejima K (1996) Metal-flow phenomena in computerized numerically controlled incremental stretch-expanding of aluminum sheets. Keikinzoku/J Jpn Inst Light Met 46:65–70
2. Jeswiet J (2001) Incremental single point forming. Trans North Am Manuf Res Inst 29:75–79
3. Filice L, Fratini L, Micari F (2002) Analysis of material formability in incremental forming. Ann CIRP 51:199–202
4. Jeswiet J, Micari F, Hirt G, Bramley A, Duflou J, Allwood J (2005) Asymmetric single point incremental forming of sheet metal. Ann CIRP 54:623–650
5. Kegg RL (1961) A new test method for determination of spinnability of metals. Trans ASME J Eng Ind Trans 83:119–124
6. Emmens WC, van den Boogaard AH (2009) An overview of stabilizing deformation mechanisms in incremental sheet forming. J Mater Process Technol 209:3688–3695
7. Allwood JM, Shouler DR, Tekkaya AE (2007) The increased forming limits of incremental sheet forming processes. Key Eng Mater 344:621–628
8. Jackson K, Allwood JM (2009) The mechanics of incremental sheet forming. J Mater Process Technol 209:1158–1174
9. Eyckens P, He S, van Bael A, van Houtte P, Duflou J (2007) Forming limit predictions for the serrated strain paths in single point incremental sheet forming. In: Cesar de Sa JMA, Santos AD (eds) NUMIFORM 2007. American Institute of Physics, Porto, pp 141–146
10. Silva MB, Skjoedt M, Atkins AG, Bay N, Martins PAF (2008) Single point incremental forming & formability/failure diagrams. J Strain Anal Eng Des 43:15–36
11. Cao J, Huang Y, Reddy NV, Malhotra R, Wang Y (2008) Incremental sheet metal forming: advances and challenges. In: Yang DY, Kim YH, Park CH (eds) ICTP 2008 International Conference on Technology of Plasticity. The Korean Society for Technology of Plasticity, Gyeongju, pp 751–752
12. Emmens WC, van den Boogaard AH (2008) Incremental forming studied by tensile tests with bending. In: Yang DY, Kim YH, Park CH (eds) ICTP 2008 International Conference on Technology of Plasticity. The Korean Society for Technology of Plasticity, Gyeongju, pp 245–246
13. Silva MB, Skjoedt M, Bay N, Martins PAF (2009) Revisiting single point incremental forming & formability/failure diagrams by means of finite elements and experimentation. J Strain Anal Eng Des 44:221–234
14. Skjoedt M, Silva MB, Martins PAF, Bay N (2008) Strain paths and fracture in multi stage single point incremental forming. In: Yang DY, Kim YH, Park CH (eds) ICTP 2008 International Conference on Technology of Plasticity. The Korean Society for Technology of Plasticity, Gyeongju, pp 239–244
15. Bambach M, Hirt G (2008) Investigation into the prediction of forming limits in incremental sheet metal forming using damage models. In: Yang DY, Kim YH, Park CH (eds) ICTP 2008 International Conference on Technology of Plasticity. The Korean Society for Technology of Plasticity, Gyeongju, pp 1777–1782
16. Atkins AG (1996) Fracture in forming. J Mater Process Technol 56:609–618
17. Rossard C (1976) Mise en forme des métaux et alliages. CNRS, Paris
18. Atkins AG (1997) Fracture mechanics and metal forming: damage mechanics and the local approach of yesterday and today. In: Rossmanith HP (ed) Fracture research in retrospect. Balkema, Rotterdam, pp 327–350
19. Skjoedt M, Silva MB, Bay N, Martins PAF, Lenau T (2007) Single point incremental forming using a dummy sheet. In: Vollertsen F, Yan S (eds) 2nd International Conference on New Forming Technology. BIAS, Bremen, pp 267–276
20. Sawada T, Fukuhara G, Sakamoto M (2001) Deformation mechanism of sheet metal in stretch forming with computer numerical control machine tools. J Jpn Soc Tech Plast 42:1067–1069